(Preprint) AAS 15-726

ORBIT DETERMINATION FOR PARTIALLY UNDERSTOOD OBJECT VIA MATCHED FILTER BANK

Timothy S. Murphy [*], Marcus J. Holzinger [†], Brien Flewelling[‡]

With knowledge of a space object's orbit, the matched filter is an image processing technique which allows low signal-to-noise ratio objects to be detected. Many space situational awareness research efforts have looked at ways to characterize the probability density function of a partially understood space object. When prior knowledge is only constrained to a probability density function, many matched filter templates could be representative of the space object, necessitating a bank of matched filters. This paper develops the measurement dissimilarity metric which is then applied to partition a general prior set of orbits. A method for hypothesis testing the result of a matched filter for a space object is developed. Finally, a framework for orbit determination based on the matched filter result is developed. Simulation shows that the analytic results enable more efficient computation and a better framework for implementing matched filters.

INTRODUCTION

Part of the current Space Situation Awareness (SAA) problem involves the orbit determination of space objects (SO). It is predicted that a new high profile collision will occur every 5 to 9 years [1]. Events like the Iridium Cosmos collision highlight the damage such events can cause [2]. Even small objects of diameter less than 10 cm which are not actively tracked still pose a threat to space assets [3]. Space and ground based electro-optical sensors (EOS) play a key role in tracking objects outside of Low Earth Orbit (LEO), where radar performance drops off. It can also be seen as an affordable alternative to radar technologies which tend to be costly [4]. Many of the small objects not already tracked by the SSN are difficult to detect due to their low strength optical signals. The ability of an EOS to reliably detect a SO in a particular image is characterized by the Signal-to-Noise Ratio (SNR) defined as the ratio of the relevant signal strength to the standard deviation of the corrupting noise. The SNR of the SO can be effectively increased by increasing the aperture of the EOS, but this tends to be costly. Coder et. al. showed that lowering the algorithm required SNR for image processing has the same sensitivity as lowering the the sensor required signal strength [5]. This research is therefore motivated to detect objects at low SNR with intelligently designed image processing techniques.

With prior information on an object, methods like rate tracking and matched filtering can provide an SNR gain for detections. The matched filter (MF) is an convolution of a known template with

[*] Graduate Student, The Guggenheim School of Aerospace Engineering, Georgia Institute of Technology, Georgia Institute of Technology North Ave NW, Atlanta, GA 30332.

[†] Assistant Professor, The Guggenheim School of Aerospace Engineering, Georgia Institute of Technology, Georgia Institute of Technology North Ave NW, Atlanta, GA 30332. AIAA Senior Member

[‡] Research Aerospace Engineer, Space Vehicles Directorate, Air Force Research Laboratory, 3550 Aberdeen Ave. SE, Kirtland AFB, NM, USA.

a measurement image. Providing the template matches the underlying signal, this provides a large SNR gain. Matched filtering originates in image and signal processing; the original formulation dates back to the 1960s as a way to detect a signal in a high noise environment [6]. It was then adapted to general image processing and moving target detection [7]. The most common implementation of a matched filter for SSA is the velocity filter which linearizes dynamics over an EOS exposure time [8]. Because rate tracking and matched filtering both provide an SNR gain at the cost of required prior knowledge, comparisons over which is better arise. Rate tracking works best on exact orbital knowledge; an imperfect rate track does not provide the same SNR Gain. If the underlying signal is unknown or partially known, a bank of matched filters can be used [9]. This approach buys better SNR gain at the expense of large computation times. It has also been shown that EOS feedback is useful via online orbit determination enabling a matched filter [10]. The problem with past use of the MF in SSA applications is that prior knowledge is treated as a binary availability. Currently, a known space object is stored as a two line element (TLE) which gives no model of uncertainty *. Many SO which either do not exist in the space object catalog or have not received updating measurements for a long time period may not be accurately described by their TLE. There have been large pushes to properly model partial knowledge through methods like admissible region and Gaussian mixture models [11] [12] [13]. The primary goal of this paper is to demonstrate the kind of sensor feedback that is possible when only partial orbit knowledge is available.

When considering an EOS attempting to measure a partially known object with low SNR, two problems are defined which will be addressed in this paper. First, how can a sensor be tasked to attempt to observe a partially known SO? This paper will approach this problem by modeling a partially known SO as a set of possible orbits. The set of possible orbits is mapped into the frame of an EOS, providing a framework to rigorously search for an object. Second, how can a sensor confidently say that a partially known SO has been detected when techniques based on exact orbital knowledge is unavailable? This problem will be addressed with a bank of matched filters based on state space partitioning. Specifically, by defining a metric for evaluating dissimilarity of the matched filter templates, the set of possible orbits can be partitioned [14]. This will enables a minimum number of matched filters to be used, while still assuring all possible orbits are represented.

Another result which this paper will develop solves a problem with MF implementation for SSA. The MF is a discrete convolution of a known signal template with the measurement image. Traditionally, this is calculated over the entire image, but for SSA, the location of a partially known SO can be bounded. Large computation times can be saved if the MF is only calculated in certain localized areas. The framework which is developed for search for partially known SO easily allows for a localized matched filter search, which this paper will include.

This paper reviews the results of a previous paper on a general approach to generating a matched filter template, and the concepts behind partitioning a set into a bank of matched filters [15]. The measurement dismilarity metric will be derived and methods for partitioning a set of orbits based on a metric will be reviewed. Orbit PDF's are converted into sets to allow this partitioning method to operate directly on the output of a linear or non-linear filter. A method to localize matched filter templates to specific parts of an image will also be developed. Some results for hypothesis testing on a MF result will be developed. An orbit determination update based on admissible regions is then integrated into this framework. Finally, a simulation based on an admissible region pass off will demonstrate the strengths of the matched filter bank method.

*spacetracks.org, last accessed Jan, 2015

The paper organization is as follows. First, this paper reviews the concept of a matched filter bank and refines the notation [15]. The, this paper will derive the measurement dissimilarity metric and review material for partitioning a set based on a metric. The localized matched filter process will then be described. Hypothesis testing and orbit determination will finish the theoretical portion of this paper. Simulations on the matched filter bank will then be included to demonstrate algorithm strengths.

PREVIOUS WORK

General Matched Filter from a Hypothesis Orbit

First, consider a particular orbit represented in position and velocity, $\mathbf{x}(t) = [\mathbf{r}^T(t)\ \dot{\mathbf{r}}^T(t)]^T$. When a particular observer is considered, any orbit can be mapped into polar coordinates around it.

$$\mathbf{x}'(t) = \mathbf{m}(\mathbf{x}(t); \mathbf{k}(t)) \tag{1}$$

where $\mathbf{x}'(t)$ is defined as

$$\begin{aligned} \mathbf{x}'(t) &= \left[\mathbf{x}_d^T(t)\ \dot{\mathbf{x}}_d^T(t)\ \mathbf{x}_u^T(t)\right]^T \\ &= \left[[\alpha(t)\ \ \delta(t)]\ [\dot{\alpha}(t)\ \ \dot{\delta}(t)]\ [\rho(t)\ \ \dot{\rho}(t)]\right]^T \end{aligned} \tag{2}$$

such that α is right ascension, δ is declination, and ρ is range. The parameter vector, $\mathbf{k}(t)$, contains information on the observer's position and velocity, along with any other parameters needed to fully define the measurement. When an EOS takes a measurement at an instantaneous time, t, only $\mathbf{x}_d(t)$ is measured.

$$\mathbf{x}_d(t) = \mathbf{h}(\mathbf{x}(t); \mathbf{k}(t)) \tag{3}$$

While $\dot{\mathbf{x}}_d$ is often reported in measurements, it is inferred from the data due to non-zero exposure time.

In reality, an EOS does not make an instantaneous measurement, but rather measures the arc through angular space, or $\mathbf{SO}(2)$. To review, $\mathbf{SO}(2)$ is the set of all bearings in $\mathbb{R}^3$, and is coordinatized by $\mathbf{x}_d$.

$$\mathbf{SO}(2) = \{\mathbf{x}_d \in [0, 2\pi) \times [-\pi/2, \pi/2)\} \tag{4}$$

The measurement arc, $\mathcal{A}_m$, can be defined as an arc through $\mathbf{SO}(2)$ which an EOS measures:

$$\begin{aligned} &\mathcal{A}_m = \{[\mathbf{x}_d^T(t)\ \ t]^T \in \mathbf{SO}(2) \times \mathbb{R} : \mathbf{x}_d(t) = \mathbf{h}(\boldsymbol{\phi}(t, t_0, \mathbf{x}(t_0)), \mathbf{k}(t)), t \in [t_0, t_0 + t_I]\} \\ &\mathcal{A}_m = \mathbf{h}(\mathbf{x}, t_0, t_I) \end{aligned} \tag{5}$$

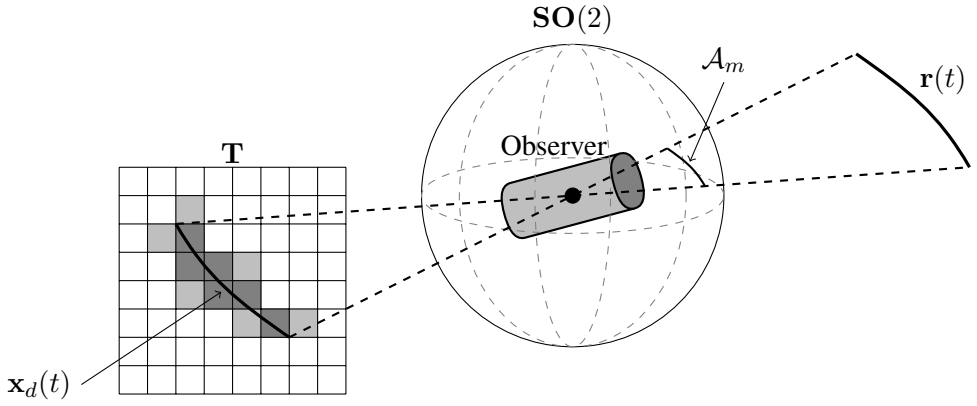

Figure 1. Modeling an optical observer in Equation 6.

To review, the flow function $\boldsymbol{\phi}(t, t_0, \mathbf{x}(t_0))$ maps an orbit from time t_0 to time t, according to orbital mechanics. The range $[t_0, t_0 + t_I]$ is the integration time of the EOS. Equation 5 uses $\mathbf{h}$ to map an orbit directly to a measurement arc. This is a slight abuse of notation; this mapping does not explicitly preserve time history. This paper assumes that when $\mathcal{A}_m$ is used, time history is known. The measurement arc and this mapping process can be visualized in Figure 1. $\mathbf{SO}(2)$ is represented by a unit sphere.

The final transformation is from a measurement arc to what is actually measured, an image. The continuous signal contained in $\mathcal{A}_m$ is integrated per pixel over the exposure time. A transformation can then be defined from the measurement arc to an actual image, $\mathbf{T}$.

$$\mathbf{T}(\mathcal{A}_m) = \mathbf{h}_T(\mathcal{A}_m) \tag{6}$$

This transformation is also illustrated in Figure 1. The notation $\mathbf{T}$ is used because this is the process by which a matched filter template can be created. If an orbit is known to sufficient precision, the measurement arc can be predicted and mapped into the pixels of an measurement frame. This predicted signal can then be used to scan for the true signal in an image.

This paper will discuss sets of measurement arcs. Typically, these will result from mapping sets of orbits through Equation 5. This paper will therefore define $\mathbb{A}$ for a given t_0, t_I as the set of all possible measurement arcs.

$$\mathbb{A} = \{\mathcal{A}_m = \mathbf{h}_i(\mathbf{x}, t_0, t_I) : \mathbf{x} \in \mathbb{R}^6\} \tag{7}$$

This is convenient for defining subsets of $\mathbb{A}$ for the measurement dissimilarity metric.

Matched Filter Bank from Partial Orbit Knowledge

A PDF is often available from orbit estimation methods. In the extreme case of object discovery, this PDF may be large, consisting of an admissible region, or a large Gaussian mixture or discrete particle distribution. Propagating this distribution through time and mapping it to an observer's sensor frame will still give a large distribution. No single measurement arc, $\mathcal{A}_m$, can be used to

represent this object; many different measurement arcs which are consistent with parts of the prior distribution could be used. It is therefore necessary to use a series of measurement arcs to feed into a matched filter.

First, define a prior set of orbits as $\mathcal{S}_0$. The most relevant application of this work is when there exists a prior PDF from some estimator or admissible region, not a set. In order to partition in equations 9 and 10, the prior information is better thought of as a set. In the case of a PDF, this could be thought of as the interior of an isoprobability surface of the PDF which is used to create this prior set, $\mathcal{S}_0$

$$\mathcal{S}_0 = \{\mathbf{x} \in \mathbb{R}^6 : f(x) \geq f_{min}\} \tag{8}$$

where the function f is the PDF. It is generally the case that a single subset set $\mathcal{S}_k \subseteq \mathcal{S}_0$ will not contain all possible orbits from a prior distribution. Any prior distribution could be partitioned into a series of subsets, $\mathcal{S}_k$. By creating s non-overlapping subsets, a partitioning can be created for any prior set, $\mathcal{S}_0$.

$$\mathcal{S}_0 = \bigcup_{k=1}^{s} \mathcal{S}_k \tag{9}$$

$$\mathcal{S}_j \cap \mathcal{S}_k = \emptyset, \forall j \neq k \tag{10}$$

It should be noted that the partitioning can overlap, and certain partitioning schemes may benefit from this condition being relaxed.

NEW THEORETICAL WORK

Admissible Region Motivating Example

As has been mentioned, the most relevant example of this methodology at this point is an admissible region, $\mathcal{AR}$. Note that the notation $\mathcal{AR}$ represents the set formed by an admissible region. A more verbose discussion of admissible regions is included in the Appendix.

$\mathcal{AR}$ is already a set and therefore does not need to be approximated as one. Each element of the set, $\mathbf{x}_u$, can be combined with the fixed $\mathbf{x}_d$, $\dot{\mathbf{x}}_d$ to form a hypothesis orbit. An admissible region is a set of orbits, which defines a prior set for a particular space object.

$$\mathcal{S}_0 = \mathcal{AR} \tag{11}$$

Therefore $\mathcal{AR}$ can be partitioned into subsets, $\mathcal{S}_k$, to enable a MF bank. Furthermore, this partitioning can be done for any observer at any time, as the admissible region can be mapped forward in time with the flow function, ϕ.

The partitions should be based on grouping orbits which produce similar templates. In application, an $\mathcal{AR}$ is often represented by a point-wise discrete approximation. For a MF bank, the most basic partition method is to create a template from each sample from the $\mathcal{AR}$. In practice, such a method is a brute force attempt which fails to take advantage of inherently redundant templates.

This paper will instead attempt to define a method to measure the similarity of templates. This will enable partitions to be defined.

The next two sections will propose a framework for creating these partitions.

Measurement Dissimilarity Metric

A bank of MF are desirable for large prior distributions, but due to computation time it is also useful to choose a minimal number of templates. This section will define a measure of template dissimilarity. As it has been shown before, the measurement arc A_m defined in Equation 5 is a mathematical equivalent to the MF template, $\mathbf{S}_0(t)$, represented by Equation 6. There could be many ways to compare similarity of measurement arcs, but a metric has many desirable properties. The most important feature of metrics which motivates this discussion is the existence of a large body of work on partitioning metric spaces. Previous work in metric spaces partitioning will be discussed [14].

The first step is to choose a metric to compare arc similarity. First, consider the similarity of two points on the celestial sphere, $\hat{\boldsymbol{\rho}}_a(t)$ and $\hat{\boldsymbol{\rho}}_b(t)$. Note that the unit vector is an equivalent representation of a point in $\mathbf{SO}(2)$. The angle between two vectors can be defined as:

$$\Delta\theta_{a,b}(t) = 2\sin^{-1}\left(\frac{||\hat{\boldsymbol{\rho}}_a(t) - \hat{\boldsymbol{\rho}}_b(t)||}{2}\right) \tag{12}$$

This particular formulation assumes $\hat{\boldsymbol{\rho}}_a(t)$, $\hat{\boldsymbol{\rho}}_b(t)$ are both unit vectors. A metric which compares two measurement arcs is desirable. Measurement arcs at an instantaneous time differ by the angle between the instantiates unit vectors, in equation 12. When considering the entire measurement arc, integrating $\Delta\theta_{a,b}(t)$ over a predefined exposure time, $[t_0, t_0 + t_I]$ takes into account how two measurement arcs differ over the relevant time interval. Thus the measurement dissimilarity metric (MDM) for a given $[t_0, t_0 + t_I]$ is defined in equation 13.

$$d_{MDM}(\hat{\boldsymbol{\rho}}_a(t), \hat{\boldsymbol{\rho}}_b(t)) = \int_{t_0}^{t_0+t_I} \Delta\theta_{a,b}(\tau)d\tau \tag{13}$$

This metric can be wrapped into the measurement arc notation. Given a particular measurement arc, $\mathcal{A}_{m,a}$, defines a time-varying unit vector, $\hat{\boldsymbol{\rho}}_a(t)$ over a predefined time interval $[t_0, t_0 + t_I]$. Therefore, the MDM can be directly computed between two measurement arcs.

$$d_{MDM}(\mathcal{A}_{m,a}, \mathcal{A}_{m,b}) = \int_{t_0}^{t_0+t_I} \Delta\theta_{a,b}(\tau)d\tau \tag{14}$$

Lemma 0.1. *The measurement dissimilarity metric defined in Equation 14 over a fixed time interval, $[t_0, t_0+t_I]$, is a metric on $\mathbb{A}$, the set of measurement arcs, for any pair $\hat{\boldsymbol{\rho}}_a(t) \in \mathcal{A}_{m,a}$, $\hat{\boldsymbol{\rho}}_b(t) \in \mathcal{A}_{m,b}$, that is, it satisfies the following:*

1. $d_{MDM}(\mathcal{A}_{m,a}, \mathcal{A}_{m,b}) \geq 0$ *(non - negativity)*

2. $d_{MDM}(\mathcal{A}_{m,a}, \mathcal{A}_{m,b}) = 0$ *if and only if* $\hat{\boldsymbol{\rho}}_a(t) = \hat{\boldsymbol{\rho}}_b(t)$ *(coincidence)*
3. $d_{MDM}(\mathcal{A}_{m,a}, \mathcal{A}_{m,b}) = d_{MDM}(\mathcal{A}_{m,b}, \mathcal{A}_{m,a})$ *(symmetry)*
4. $d_{MDM}(\mathcal{A}_{m,a}, \mathcal{A}_{m,c}) \leq d_{MDM}(\mathcal{A}_{m,a}, \mathcal{A}_{m,b}) + d_{MDM}(\mathcal{A}_{m,b}, \mathcal{A}_{m,c})$ *(triangle inequality)*

Proof. Non negativity follows directly from the range of the functions involved.

$$
\begin{aligned}
||\hat{\boldsymbol{\rho}}_a - \hat{\boldsymbol{\rho}}_b|| &\in [0, 2] \\
\sin^{-1}(\frac{||\hat{\boldsymbol{\rho}}_a(t) - \hat{\boldsymbol{\rho}}_b(t)||}{2}) &\in [0, \pi/2] \\
\Delta\theta_{a,b}(t) &\geq 0 \\
\int_{t_0}^{t_0+t_I} \Delta\theta_{a,b}(t)dt &\geq 0
\end{aligned}
\tag{15}
$$

For coincidence, first note that $f(t) = 0, t \in [t_1, t_2] \implies \int_{t_1}^{t_2} f(t)dt = 0, \ \forall t \in [t_1, t_2]$, for any continuous function $f(t)$ and arbitrary values of t_1 and t_2. Next, note that over the range of inputs, $x \in [0, 1], \sin^{-1}(x) = 0 \iff x = 0$. This directly implies 2. This is equivalent to saying the only way the measurement dissimilarity metric can be zero is if the measurement arcs are identical.

For symmetry, note that $||\hat{\boldsymbol{\rho}}_a - \hat{\boldsymbol{\rho}}_b|| = ||\hat{\boldsymbol{\rho}}_b - \hat{\boldsymbol{\rho}}_a||$ for an arbitrary pair of unit vectors. 3 follows immediately.

The shortest distance along the surface of a sphere between two points is the orthodromic distance. This comes directly from the way the great circle distance is derived. Therefore $\Delta\theta_{a,c}(t) \leq \Delta\theta_{a,b}(t) + \Delta\theta_{b,c}(t)$ must be true, because $\Delta\theta_{a,b}(t) + \Delta\theta_{b,c}(t)$ represents another path along the surface of a sphere from a to c. Remember the following property of integrals

$$
f_a(t) \leq f_b(t) \Rightarrow \int_{t_1}^{t_2} f_a(t)dt \leq \int_{t_1}^{t_2} f_b(t)dt
$$

which is true for any t_1 and t_2. This gives the triangle inequality.

$$
\int_{t_0}^{t_0+t_I} \Delta\theta_{a,c}(t)dt \leq \int_{t_0}^{t_0+t_I} \Delta\theta_{a,b}(t)dt + \int_{t_0}^{t_0+t_I} \Delta\theta_{b,c}(t)dt \tag{16}
$$

□

Thus, the MDM is a metric on $\mathbb{A}$, the set of measurement arcs, allowing partition methods to be applied to $\mathbb{A}$. The desired partitioning will, however, be occurring on orbits which exist as elements in $\mathbb{R}^6$. The MDM can also be defined over a set of orbits because of the onto mapping from orbits to measurement arcs, Equation 5. This can also be shown by acknowledging that $\hat{\boldsymbol{\rho}}_a(t)$ is a function of $\mathbf{x}(t)$.

$$\Delta\theta_{a,b}(t) = 2\sin^{-1}\left(\frac{||\hat{\boldsymbol{\rho}}_a(\mathbf{x}(t)) - \hat{\boldsymbol{\rho}}_b(\mathbf{x}(t))||}{2}\right)$$
$$d_{MDM}(\mathbf{x}_a, \mathbf{x}_b) = \int_{t_0}^{t_0+t_I} \Delta\theta_{a,b}(\tau)d\tau \tag{17}$$

The following corollary will show that the MDM is a pseudo-metric on $\mathbb{R}^6$, or any set of orbits.

Corollary 0.2. *The measurement dissimilarity metric defined in Equation 13 over a fixed time interval, $t \in [t_0, t_0 + t_I]$, is a pseudo-metric on $\mathbb{R}^6 \times \mathbb{R}$ for any pair of orbits $\mathbf{x}_a(t), \mathbf{x}_b(t)$, that is, it satisfies the following:*

1. $d_{MDM}(\mathbf{x}_a(t), \mathbf{x}_b(t)) \geq 0$ *(non - negativity)*
2. $d_{MDM}(\mathbf{x}_a(t), \mathbf{x}_b(t)) = d_{MDM}(\mathbf{x}_b(t), \mathbf{x}_a(t))$ *(symmetry)*
3. $d_{MDM}(\mathbf{x}_a(t), \mathbf{x}_c(t)) \leq d_{MDM}(\mathbf{x}_a(t), \mathbf{x}_b(t)) + d_{MDM}(\mathbf{x}_b(t), \mathbf{x}_c(t))$ *(triangle inequality)*

Proof. Non negativity and symmetry follow from Lemma 0.1. Every orbit will map to a measurement arc which exists on $\mathbb{A}$.

First fix three orbits, $\mathbf{x}_a$, $\mathbf{x}_b$, and $\mathbf{x}_c$. Because the mapping from orbits to measurement arcs is onto, these orbits map to single time-varying unit vectors, $\hat{\boldsymbol{\rho}}_a(t)$, $\hat{\boldsymbol{\rho}}_b(t)$, and $\hat{\boldsymbol{\rho}}_c(t)$. The triangle inequality follows from Lemma 0.1. □

The pseudo-metric does not have a coincidence property because the mapping from orbits to measurement arcs is not one-to-one. However, this section will discuss metrics rather than psuedo-metrics. In order to enable metric space partitioning based on pseudo-metrics, coincident objects are considered as one object [16]. This is equivalent to saying all orbits that produce the identically same streak are the same object.

The properties of a metric seem obvious and trivial at first glance, but in fact a wide variety of partition methods exist. A good discussion of metric based search and partition methods can be found in the text *Similarity Search: The Metric Space Approach* by Zezula et al. [14]. An overview of the concepts and methods will be discussed here. The broad approach falls into two categories, ball partition (BP) methods and generalized hyperplane tree (GHT) methods [17] [16]. The literature is rich with implementations of these methods.

BP is the first method and is based around a predetermined a maximum distance, d_{max}. It can be visualized in Figure 2(a). d_{max} can be defined as a maximum dissimilarity of two measurements before their templates are considered unique. Once a d_{max} is set, BP is straightforward. BP is implemented by choosing a series of pivot point, $x_k \in \mathcal{S}_0$. Each partition $\mathcal{S}_k$ is a ball centered at a respective pivot, x_k, with a radius d_{max}

$$\mathcal{S}_k = \{x \in \mathcal{S}_0 : d_{MDM}(x, x_k) \leq d_{max}\} \tag{18}$$

The second method is analogous to the Voronoi diagram. It can be visualized in Figure 2(b). The generalized hyperplane tree (GHT) is implemented by setting a number of pivots and then binning

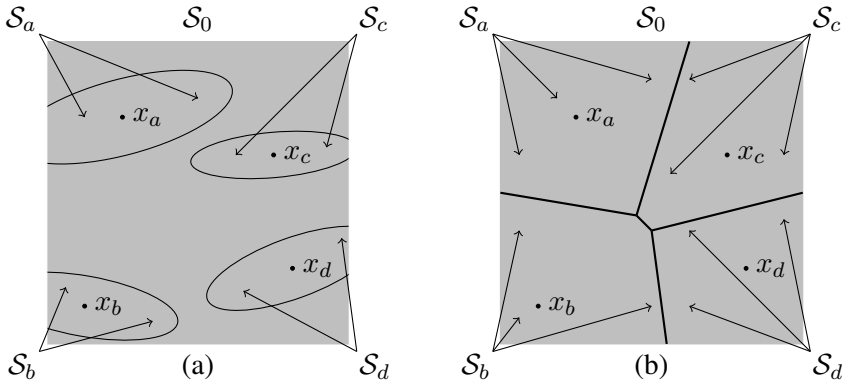

Figure 2. Ball partition and generalized hyperplane methods [14]

the rest of the space by defining hyperplanes of equal metric distance from each pair of pivots. Each partition is then the set of points which are closer to a particular pivot than any other pivot.

$$\mathcal{S}_a = \{x \in \mathcal{S}_0 : d_{MDM}(x, x_a) \leq d_{MDM}(x, x_k), \forall k \neq a\} \tag{19}$$

The goal of this paper is not to provide an indepth analysis of partition methods. The results in this work use the BP method to partition prior sets. The best choice for a partition method is application dependent.

Localization of Matched Filter

The matched filter involves a discrete convolution of the template over the measurement image. The matched filter can be applied over the entire measurement image, but is a computationally costly process. If certain templates can be skipped or searched in only a local area, large computation times are saved. This section will define a method by which the partition sets can be used to localize the matched filter search.

When a particular hypothesis orbit is mapped into the sensor frame, $\mathcal{A}_m$ has an associated location in that frame. Each partition $\mathcal{S}_k$, as defined, is a set of hypothesis orbits. If a particular anchor time, t^*, is defined a particular partition can be mapped into $\mathbf{SO}(2)$.

$$\mathcal{S}'_k = \{\mathbf{x}_d \in \mathbf{SO}(2) : \mathbf{x}_d = \mathbf{h}(\boldsymbol{\phi}(t^*; t_0, \mathbf{x}(t_0)), \mathbf{k}(t_0)), \mathbf{x}(t_0) \in \mathcal{S}_k, \} \tag{20}$$

For this particular partition's template to be necessary, the observer must be looking at the object during the exposure time.

$$\mathcal{O}_i = \{\mathbf{x}_d \in \mathbf{SO}(2) : \mathbf{x}_d \text{ in observer frame at } t^*\} \tag{21}$$

When a MF template is used to search an image, it is tiled over the pixels. This is done by choosing an anchor pixel in the template, typically the center pixel. This anchor pixel is aligned

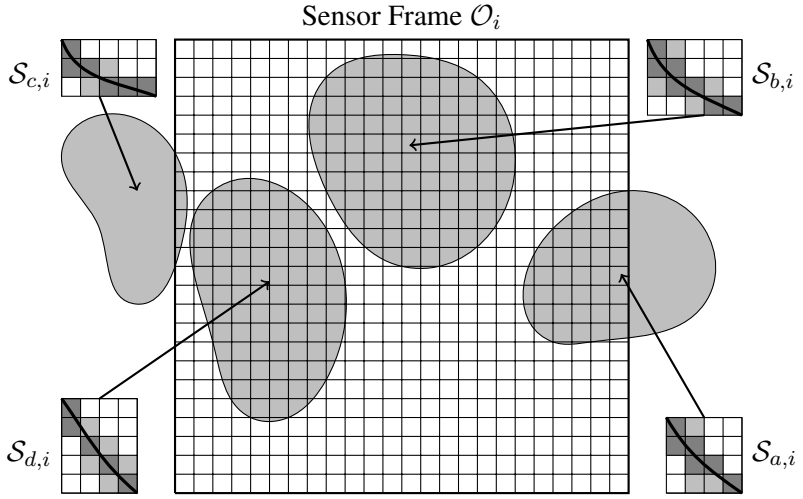

Figure 3. Localized searching of the sensor frame for partitions a through d

with each pixel in the image and then the convolution is evaluated. $\mathcal{S}'_k$ is the set of all unit vectors which can be generated from the partition set $\mathcal{S}_k$ at t^*. If the anchor pixel is defined as the location of the object at t^*, a search space can be defined

$$\mathcal{S}_{k,i} = \mathcal{O}_i \cap \mathcal{S}'_k \tag{22}$$

$\mathcal{S}_{k,i}$ represents the search space for template k in an image taken by observer i. This can be seen in Figure 3, where each template has local areas where it should be evaluated.

This method will yield one of two results. First, $\mathcal{S}_{k,i}$ can be empty, in which case the template does not require searching for a particular image. Second, $\mathcal{S}_{k,i}$ is non-empty, and the template need only be searched over a subset of $\mathcal{O}_i$. More generally, this illustrates a fundamental problem of searching for partially known SO: the search space defined by prior knowledge can be larger than what can be captured by a single measurement. The prior set, $\mathcal{S}_0$, and the subsets, $\mathcal{S}'_k$ can inform sensor tasking. For example, a tasking scheme could be to take a minimum number of observations to observe the entire set, $\mathcal{S}_0$. Tasking schemes for observing partially known space objects based on this framework is considered future work.

Probability of Detection and Likelihood Map from Matched Filter

Consider a matched filter template which consists of n non-zero pixels a_j. When calculating the matched filter for a particular position, each pixel in the template is associated with a particular measurement pixel, z_j. Then the matched filter correlation is calculated by

$$z_{MF} = \sum_{j=1}^{n} a_j z_j \tag{23}$$

Next, assume that the pixels consist of some signal and mean zero Gaussian read noise.

$$z_j = s_j + w_j \tag{24}$$
$$w_j \approx \mathcal{N}(0, \sigma_w) \tag{25}$$

Note that in this formulation, s_j is equivalent to the mean of the measurement z_j. In order to have zero mean read noise in practice, an effective background subtraction method is needed to remove artifacts including dark current, and hot pixels. Next, consider the null and test hypotheses, for a single pixel, z_j.

$$\begin{aligned} H_0 &: s_j = 0 \\ H_1 &: s_j > 0 \end{aligned} \tag{26}$$

which is equivalent to a test on the mean of a Gaussian random variable. This sets up a hypothesis test for if a particular pixel contains any signal, or if what is measured is solely due to noise. Using the test variable, z_j, an acceptable probability of false alarm can be chosen, P_{FA}, and a p-value, p_j can be calculated.

$$p_j = 1 - f_{CDF}(z_j, \sigma_w) \tag{27}$$

where f_{CDF} is the evaluation of the cumulative density function (CDF) of a gaussian distibution with standard deviation, σ_w.

In reality, the hypothesis test should be if the series of pixels tested by the matched filter all have non zero signal. The formulation of these hypotheses on the matched filter is:

$$\begin{aligned} H_0 &: \exists\ j \in [1, \ldots, n] : s_j = 0 \\ H_1 &: s_j > 0\ \forall\ j \in [1, \ldots, n] \end{aligned} \tag{28}$$

This test is less straight forward to evaluate. There exist methods such as Fisher's method for evaluating a particular hypothesis test multiple times. Fisher's method defines the following test statistic:

$$\tilde{z} = -2 \sum_{j=1}^{n} \ln(p_j) \approx \chi^2_{2k} \tag{29}$$

This new test statistic, belonging to a chi squared distribution, approximately evaluates the combined hypothesis. This hypothesis test can be used to determine is there is significant evidence that the predicted signal exists in the predicted location. This test statistic is part of an ongoing research effort, and more work is needed define a "best" method.

Orbit Determination Based Primed by Admissible Region

The main motivating case for this research is an admissible region hand off for fast and accurate orbit determination. The basic case of this is trivial; if two observers with geometrically diverse locations observe a SO, the exact position can be triangulated [18]. For the case of observers at different times and positions attempting to perform orbit determination on a particular space object, more analysis is needed. First, consider the previously laid out matched filter bank, preformed on an admissible region detected by observer i, $\mathcal{AR}_i$. This admissible region can be propagated forward to time t_0, forming $\mathcal{S}_0$ and mapped into the sensor frame of a second observer j. If a statistically significant detection is made by the matched filter bank, a measurement can be made. This measurement, made by observer j, will consist of the determinable states for an EOS:

$$\mathbf{x}'_{d,j}(t_0) = [\alpha(t_0), \delta(t_0), \dot{\alpha}(t_0), \dot{\delta}(t_0)]^T \tag{30}$$

If the calculated $\mathbf{x}'_{d,j}(t_0)$ is not consistent with the location and rate of the template used to detect it, then the measurement can be disregarded; the object that has been detected is not consistent with any hypothesis generated from $\mathcal{S}_0$. Assuming, the measurement and template are consistent, an admissible region, $\mathcal{AR}_j$, can be constructed. Now, there exists two sets $\mathcal{S}_0$ and $\mathcal{AR}_j$ both represented by orbits at a particular time, t_0. Furthermore, it is known that both admissible regions contain an orbit consistent with a particular measurement, $\mathbf{x}'_{d,j}(t_0)$. This implies a non zero intersection of the two admissible regions, that is,

$$\mathcal{S}_0 \cap \mathcal{AR}_j \neq \emptyset \tag{31}$$

Fujimoto and Scheeres showed that if two arbitrary admissible region intersect, there is a diminishingly low probability that they were not generated from the same object [19]. This statement implies that whatever orbit(s) in $\mathcal{S}_0$ that could create the measurement $x_{d,j}(t_0)$, are the intersection of these two admissible regions, and the probable correct orbit. The Fujimoto and Scheeres paper works with exact admissible regions and draws the conclusion that the intersection must necessarily be a single point in the state space. This paper must assume uncertainties in the measurements of $\mathcal{S}_0$ and $\mathcal{AR}_j$, implying a non-point intersection.

$$\mathcal{S}'_0 = \mathcal{S}_0 \cap \mathcal{AR}_j \tag{32}$$

where $\mathcal{S}'_0$ is a new prior information set. The uncertainty in $\mathcal{S}_0$ can be represented by a variety of methods, including Gaussian mixture models [13], [20].

$$P(\mathbf{x}(t_0)|\mathcal{S}_0) = P(\mathcal{S}_0) \tag{33}$$

The new measurement defines a Bayesian update

$$P(\mathbf{x}|\mathbf{x}'_{d,j}(t_0)) = \frac{P(\mathbf{x}'_{d,j}(t_0)|\mathbf{x})P(\mathbf{x}|\mathcal{S}_0)}{P(\mathbf{x}'_{d,j}(t_0))} \tag{34}$$

a (m)	e	Ω (rad)	i (rad)	ω (rad)	f (rad)
1.2658e+04	0.2198	2.3863	0.3489	1.2698	0.3724

Table 1. orbital elements for simulation

The measurement likelihood map, $P(\mathbf{x}'_{d,j}(t_0)|\mathbf{x})$, can be calculated from the localization of $x_{d,j}(t_0)$. The localization of $x_{d,j}(t_0)$ must necessarily be calculated from the matched filter result, which is represented by the hypothesis test 28.

$$P(\mathbf{x}'_{d,j}(t_0)|\mathbf{x}) = P(z_j > 0 \ \forall \ j \in [1, \ldots, n]) \tag{35}$$

This implies that the matched filter can be built into a Bayesian filter update, allowing the matched filter bank to be built into a particle-based filter.

The new prior set, $\mathcal{S}'_0$, can be approximated by $\mathcal{R}_i \cap \mathcal{R}_j$. Note that by definition $\mathcal{S}_0 \supseteq \mathcal{S}_0 \cap \mathcal{R}_j$, implying that this calculation consists only of deleting parts of $\mathcal{S}_0$. The knowledge obtained from $\mathbf{x}'_{d,j}(t_0)$ can be used to rate track the object or inform an online matched filter [10].

SIMULATION RESULTS

A medium earth orbiting object, with parameters in Table 1 is simulated to demonstrate the admissible region hand off. An observer, $\mathbf{o}_1$, located in Colorado, takes an observation of the space object at time $t_0 = 0$, and an admissible region is generated. The SO and observer position and velocities for the simulation are:

$$\begin{aligned}
\mathbf{r} &= [-5906.3 \ \ -7313.5 \ \ 3410.0]^T (km) \\
\dot{\mathbf{r}} &= [5.0791 \ \ -4.7364 \ \ -0.0121]^T (km/s) \\
\mathbf{o}_1 &= [-1210.1 \ \ -4740.1 \ \ 4092.4]^T (km) \\
\dot{\mathbf{o}}_1 &= [0.3447 \ \ -0.0880 \ \ 0.0]^T (km/s)
\end{aligned}$$

The admissible region through out these simulation results is represented by a discrete point-wise approximation. The particles are generating by sampling random particles in ranges and range rate space, and enforcing the admissible region constraints to throw out particles. This admissible region is approximated by 5000 particles. The admissible region is visualized in figure 4.

A second observer, $\mathbf{o}_2$, located in California, takes a second observation of the SO, also at $t_0 = 0$. The second observer has the following parameters:

$$\begin{aligned}
\mathbf{o}_2 &= [-5467.7 \ \ -2383.1 \ \ 2259.7]^T (km) \\
\dot{\mathbf{o}}_2 &= [0.1733 \ \ -0.3976 \ \ 0.0]^T (km/s)
\end{aligned}$$

The measurement is an image with the SO located at the center of the image. The image is generated with a 10 second exposure time, field of view of 10 degrees, and sidereal stare Con Ops.

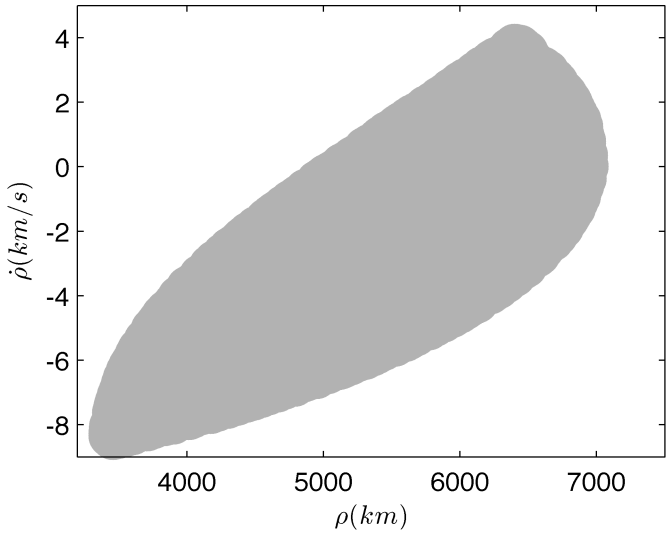

Figure 4. Admissible region in range and range rate space.

The object is obscured by significant noise, giving a peak, pixel-wise SNR of 0.86. Note that as the name implies, this SNR is calculated by the signal strength for a single pixel over the standard deviation of the noise for that pixel. The measurement image is shown in Figure 5.

In order to give qualitative insight into the computational cost of the ball partitioning, the simulation has been run for a range of MDM threshold values. The peak SNR gain, number of templates, and the computation time are plotted on a semi-log scale in Figure 6. In part (a) of Figure 6, the SNR gain is shown to vary more significantly with a higher MDM threshold. Because raw measurement SNR is constant, a perfect template should always provide the same SNR gain. A small MDM threshold will provide larger numbers of partitions which reliably find a perfect partition. As the number of templates falls, a near perfect template is not always found and the SNR gain becomes more variable. It should be noted that the SNR gain for high MDM does not follow a trend; perfect

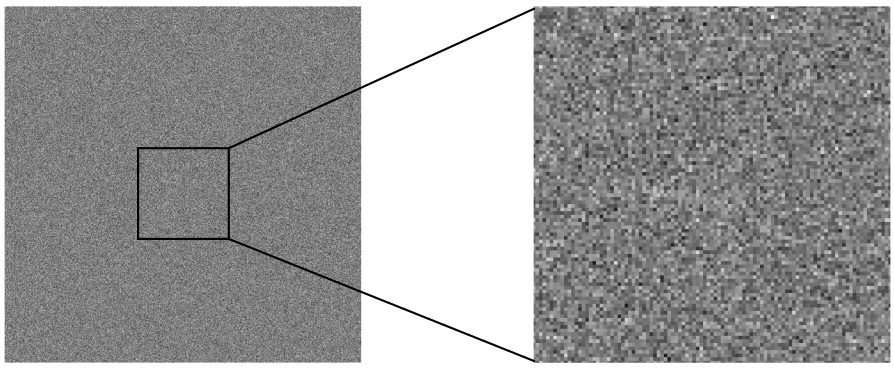

Figure 5. Measurement Image taken by observer 2

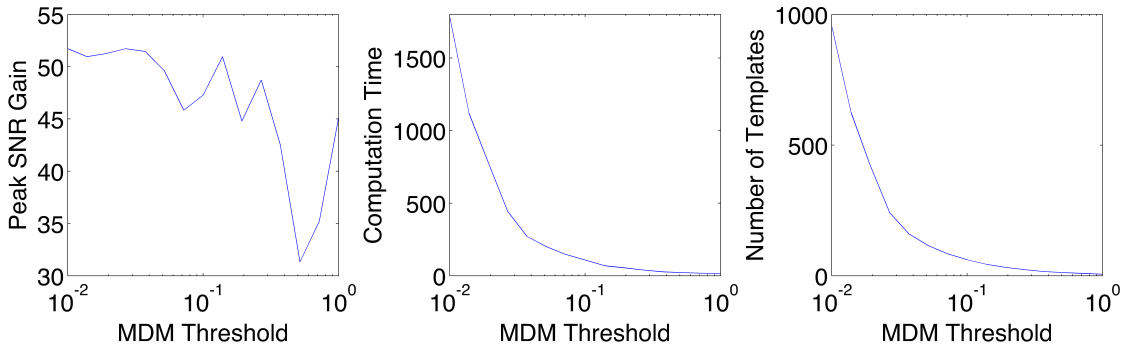

Figure 6. Results from varying MDM threshold.

Figure 7. Sampling of matched filter templates from partitioning.

templates can be found but are less likely. Computation time follows a predictable curve; more templates proportionately leads to more computation time.

The measurement arc is calculated for each particle, which gives 5000 hypothesis matched filter templates. The measurements arcs are represented by a time series of unit vectors. A ball partitioning algorithm sorts the particles into subsets containing consistent orbits. A maximum MDM value of $d_{max} = 0.1\ rad \cdot s$ is chosen; more work on this topic is needed to establish a "best" MDM threshold. The partitioning provides 60 distinct partitions with corresponding templates. Figure 7 shows a sample of the types of templates which are generated.

The templates with corresponding partitions are searched in the image. The matched filter gives a value for each pixel in the image which the template is centered at. The standard deviation of the matched filter on a signal composed only of noise gives an analytic value for the post filter standard deviation. This allows SNR to be calculated for each pixel. The results are displayed as an image of post filter SNR with peak pixel-wise SNR Gain. A larger gain implies the presence of a signal inconsistent with noise. Figure 8 shows the correlation maps for three templates. 8.a shows an incorrect template which doesn't produce significant SNR gain. 8.b shows a template with an imperfect template, illustrating the kind of SNR gain possible in real operation. 8.c shows a template primed with perfect orbital knowledge, simply to illustrate what the ideal case can look like.

After the correlation is calculated, the SO orbit can be estimated. Using the new measurements, the PDF over the original admissible region can be approximated. This was done using a simple Gaussian uncertainty update for each of the particles, and can be seen in Figure 9. Comparing Figures 4 and 9 illustrates the increases confidence in the orbit location.

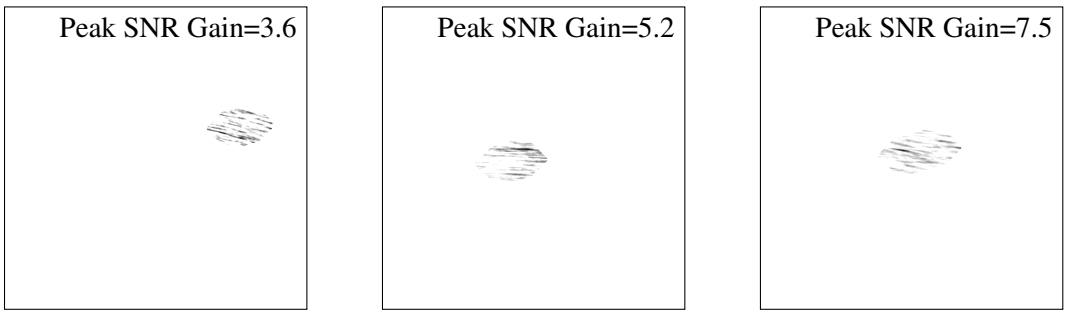

(a) Incorrect Template SNR Map (b) Similar Template SNR Map (c) Perfect Template SNR Map

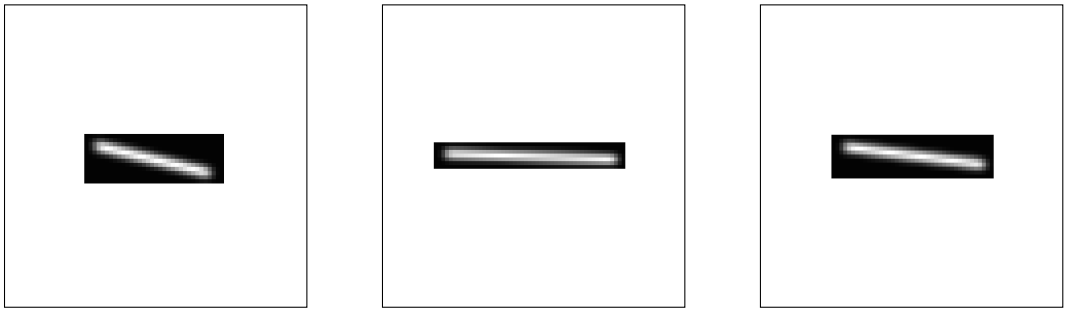

(d) Incorrect Template (e) Similar Template (f) Perfect Template

Figure 8. Correlation results from a variety of templates

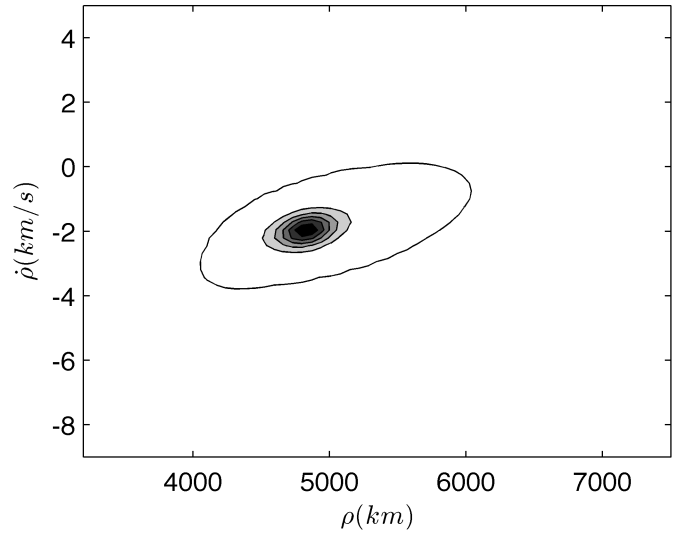

Figure 9. Post measurement PDF

CONCLUSIONS

It has been shown that the matched filter can be formulated as a bank of filters based on partial prior knowledge. This bank provides SNR gain, allowing measurements to be taken for dim SO that would normally be undetectable. Intelligent localization of the matched filter on a particular image can save processing time. The matched filter bank can lead to significant increases in orbital knowledge, and orbit determination.

ACKNOWLEDGMENTS

We would like to thank the AFRL Scholars Program for partially supporting this project. We would also like to thank Brad Sease for providing help with hypothesis tests for matched filters.

REFERENCES

[1] J. Liou, "Modeling the Large and Small Orbital Debris Populations for Environment Remediation," 2013.

[2] T. Kelso *et al.*, "Analysis of the iridium 33 cosmos 2251 collision," tech. rep., Center for Space Standards & Innovation, 2009.

[3] A. Rossi, "The earth orbiting space debris," *Serbian Astronomical Journal*, Vol. 170, No. 1, 2005, pp. 1–12, 10.2298/saj0570001r.

[4] M. D. Morales, "Space Fence program awards contracts for concept development," July 2009.

[5] R. D. Coder and M. J. Holzinger, "Multi-Objective Design of Optical Systems for Space Situational Awareness," *Advances in Space Research*, 2015, submitted.

[6] D. O. North, "An analysis of the factors which determine signal/noise discrimination in pulsed-carrier systems," *Proceedings of the IEEE*, Vol. 51, No. 7, 1963, pp. 1016–1027, 10.1109/proc.1963.2383.

[7] I. Reed, R. Gagliardi, and H. Shao, "Application of three-dimensional filtering to moving target detection," *Aerospace and Electronic Systems, IEEE Transactions on*, Vol. AES-19, No. 6, 1983, pp. 898–905, 10.1109/taes.1983.309401.

[8] M. Levesque, "Automatic reacquisition of satellite positions by detecting their expected streaks in astronomical images," *Proceedings of the Advanced Maui Optical and Space Surveillance Technologies Conference*, 2009, p. E81.

[9] M. Dragovic, "Velocity filtering for target detection and track initiation," tech. rep., DTIC Document, 2003.

[10] B. Sease, T. Murphy, B. Flewelling, M. J. Holzinger, and J. Black, "Enabling direct feedback between initial orbit determination and sensor data processing for detection and tracking of space objects," *SPIE Defense+ Security*, International Society for Optics and Photonics, 2015, pp. 94690M–94690M, 10.1117/12.2181980.

[11] A. Milani, G. F. Gronchi, M. d. Vitturi, and Z. Knežević, "Orbit determination with very short arcs. I admissible regions," *Celestial Mechanics and Dynamical Astronomy*, Vol. 90, No. 1-2, 2004, pp. 57–85.

[12] D. Farnocchia, G. Tommei, A. Milani, and A. Rossi, "Innovative methods of correlation and orbit determination for space debris," *Celestial Mechanics and Dynamical Astronomy*, Vol. 107, No. 1-2, 2010, pp. 169–185, 10.1007/s10569-010-9274-6.

[13] K. J. DeMars and M. K. Jah, "Probabilistic initial orbit determination using gaussian mixture models," *Journal of Guidance, Control, and Dynamics*, Vol. 36, No. 5, 2013, pp. 1324–1335.

[14] P. Zezula, G. Amato, V. Dohnal, and M. Batko, *Similarity search: the metric space approach*, Vol. 32. Springer Science & Business Media, 2006, 10.1007/0-387-29151-2.

[15] T. S. Murphy, B. Flewelling, and M. J. Holzinger, "Particle and Matched Filtering using Admissible Regions," *AAS/AIAA Space Flight Mechanics Meeting*, 2015.

[16] E. Chávez, G. Navarro, R. Baeza-Yates, and J. L. Marroquín, "Searching in metric spaces," *ACM computing surveys (CSUR)*, Vol. 33, No. 3, 2001, pp. 273–321, 10.1145/502807.502808.

[17] J. K. Uhlmann, "Satisfying general proximity/similarity queries with metric trees," *Information processing letters*, Vol. 40, No. 4, 1991, pp. 175–179, 10.1016/0020-0190(91)90074-r.

[18] B. Sease, K. Schmittle, and B. Flewelling, "MULTI-OBSERVER RESIDENT SPACE OBJECT DISCRIMINATION AND RANGING," *AAS/AIAA Space Flight Mechanics Meeting*, 2015.

[19] K. Fujimoto and D. J. Scheeres, "Applications of the admissible region to space-based observations," *Advances in Space Research*, Vol. 52, No. 4, 2013, pp. 696–704.

[20] J. L. Worthy III and M. J. Holzinger, "Incorporating Uncertainty in Admissible Regions for Uncorrelated Detections," *Journal of Guidance, Control, and Dynamics*, Vol. 0, No. 0, 2015, pp. 1–17, 10.2514/1.g000890.

[21] G. Tommei, A. Milani, and A. Rossi, "Orbit determination of space debris: admissible regions," *Celestial Mechanics and Dynamical Astronomy*, Vol. 97, No. 4, 2007, pp. 289–304, 10.1007/s10569-007-9065-x.

ADMISSIBLE REGIONS REVIEW

A typical optical measurement of a space object contains good knowledge of angle and angle rates known as observable states, $\mathbf{x}_d \in \mathbb{R}^4$. An orbit requires six disparate data types to be fully constrained. Historically, the final two data types are angle accelerations or range and range rate (from radar data). This AR formulation uses range and range rate as the final two states, known as

undetermined states $\mathbf{x}_u \in \mathbb{R}^2$. It is assumed that no information can be reliably used to determine these states from measurements. The following notation was developed by Worthy et al [20]. Using equations (1) and (3) and the fact that the measurement cannot be dependent on $\mathbf{x}_u$, the following measurement function can be written.

$$\mathbf{y}(t) = \mathbf{h}(\mathbf{x}_d; \mathbf{k}, t) \tag{36}$$

Furthermore, this implies a one to one and onto relationship between $\mathbf{y}(t)$ and $\mathbf{x}_d$

$$\mathbf{x}_d = \mathbf{h}^{-1}(\mathbf{y}; \mathbf{k}, t) \tag{37}$$

An AR is then created by enforcing a series of constraints of the form

$$g_i(\mathbf{x}_d, \mathbf{x}_u; \mathbf{k}, t) \leq 0 \tag{38}$$
$$g_i(\mathbf{h}^{-1}(\mathbf{y}; \mathbf{k}, t), \mathbf{x}_u; \mathbf{k}, t) \leq 0 \tag{39}$$

It should be noted that these constraints can be thought of as hypotheses. The AR is then the space where all hypotheses are true. Next, we define an admissible region, $\mathcal{AR}_i \in \mathbb{R}^2$, predicated on g_i

$$\mathcal{AR}_i := \left\{ \mathbf{x}_u | g_i(\mathbf{h}^{-1}(\mathbf{y}; \mathbf{k}, t), \mathbf{x}_u; k, t) \leq 0 \right\} \tag{40}$$

In practice, an admissible region predicated on n constraints is used.

$$\mathcal{AR} = \bigcap_{i=1}^{n} \mathcal{AR}_i \tag{41}$$

Next, the two most common constraints are defined. For optical observer AR, the primary constraint typically considered is that of Earth-orbiting SO, defined as $g_{\mathcal{E}}$. There exists a derivation to show the following equations represent energy as a function of $[\rho, \dot{\rho}]$ and known parameters. The following results were originally derived for Earth objects by Tommei et al [21]. $\mathcal{E}$ is the orbital energy, which must be negative for an Earth-orbiting SO.

$$2\mathcal{E} = g_{\mathcal{E}}(\mathbf{h}^{-1}(\mathbf{y}; \mathbf{k}, t), \mathbf{x}_u; \mathbf{k}, t) \leq 0 \tag{42}$$
$$2\mathcal{E} = \dot{\rho}^2 + w_1 \dot{\rho} + T(\rho) - \frac{2\mu}{\sqrt{S(\rho)}} \leq 0 \tag{43}$$
$$T(\rho) = w_2 \rho^2 + w_3 \rho w_4 \tag{44}$$
$$S(\rho) = \rho^2 + w_5 \rho + w_0 \tag{45}$$

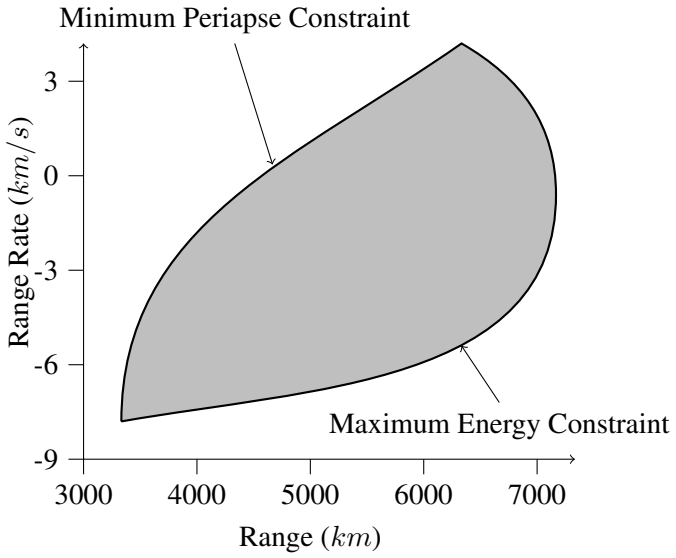

Figure 10. Sample admissible region

where the constants w_{0-5} are functions of the parameter vector, $\mathbf{k}$, defined as

$$w_0 = ||\mathbf{o}||^2 \tag{46}$$
$$w_1 = 2\dot{\mathbf{o}} \cdot \hat{\boldsymbol{\rho}} \tag{47}$$
$$w_2 = \dot{\alpha}^2 \cos^2\delta + \dot{\delta} \tag{48}$$
$$w_3 = 2(\dot{\alpha}\dot{\mathbf{o}} \cdot \hat{\boldsymbol{\rho}}_{\boldsymbol{\alpha}} + \dot{\delta}\dot{\mathbf{o}} \cdot \hat{\boldsymbol{\rho}}_{\boldsymbol{\delta}}) \tag{49}$$
$$w_4 = ||\dot{\mathbf{o}}||^2 \tag{50}$$
$$w_5 = 2\mathbf{o} \cdot \hat{\boldsymbol{\rho}} \tag{51}$$

where $\mathbf{o}$ and $\dot{\mathbf{o}}$ are the position and velocity of the observer, $\hat{\boldsymbol{\rho}}$ is the unit vector from the angles, and $\hat{\boldsymbol{\rho}}_\alpha$ and $\hat{\boldsymbol{\rho}}_\delta$ are given by

$$\hat{\boldsymbol{\rho}} = [\cos\alpha\cos\delta \quad \sin\alpha\cos\delta \quad \sin\delta]^T \tag{52}$$
$$\hat{\boldsymbol{\rho}}_{\boldsymbol{\alpha}} = [-\sin\alpha\cos\delta \quad \cos\alpha\cos\delta \quad 0]^T \tag{53}$$
$$\hat{\boldsymbol{\rho}}_{\boldsymbol{\delta}} = [-\cos\alpha\sin\delta \quad -\sin\alpha\sin\delta \quad \cos\delta]^T \tag{54}$$

A second commonly used constraint is g_r, a constraint on the radius of perigee. There exists a analytic derivation for the following [12]. It should be noted that $\mathbf{D}$, $\mathbf{E}$, $\mathbf{F}$, and $\mathbf{G}$ are vector quantities.

$$g_r(\rho, \dot{\rho}, \mathbf{x}_d; \mathbf{k}) = (r_{min}^2 - \|\mathbf{D}\|^2)\dot{\rho} - P(\rho)\dot{\rho} - U(\rho) + r_{min}^2 T(\rho) - \frac{2r_{min}\mu}{\sqrt{S(\rho)}} \leq 0 \tag{55}$$

$$P(\rho) = 2\mathbf{D} \cdot \mathbf{E}\rho^2 + 2\mathbf{D} \cdot \mathbf{F}\rho + 2\mathbf{D} \cdot \mathbf{G} - r_{min}^2 w_1 \tag{56}$$

$$U(\rho) = \|\mathbf{E}\|^2\rho^4 + 2\mathbf{E} \cdot \mathbf{F}\rho^3 + (2\mathbf{E} \cdot \mathbf{G} + \|\mathbf{F}\|^2)\rho^2 + 2\mathbf{F} \cdot \mathbf{G}\rho + \|\mathbf{G}\|^2 - 2r_{min}\mu \tag{57}$$

where the $\mathbf{D}$, $\mathbf{E}$, $\mathbf{F}$, and $\mathbf{G}$ are defined as

$$\mathbf{D} = \mathbf{q} \times \hat{\boldsymbol{\rho}} \tag{58}$$

$$\mathbf{E} = \hat{\boldsymbol{\rho}} \times (\dot{\alpha}\hat{\boldsymbol{\rho}}_\alpha + \dot{\delta}\hat{\boldsymbol{\rho}}_\delta) \tag{59}$$

$$\mathbf{F} = \mathbf{q} \times (\dot{\alpha}\hat{\boldsymbol{\rho}}_\alpha + \dot{\delta}\hat{\boldsymbol{\rho}}_\delta) + \hat{\boldsymbol{\rho}} \times \dot{\mathbf{q}} \tag{60}$$

$$\mathbf{G} = \mathbf{q} \times \dot{\mathbf{q}} \tag{61}$$

More ways exist to further constrain an admissible region. Beyond perigee and energy, any further restriction typically requires an assumption about the object. For example, if the object being observed is known to be near a GEO, constraints could be placed on semi major axis or eccentricity. This can enable prior orbital knowledge to be used to enhance convergence.